NICOLAUS COPERNICUS UNIVERSITY IN TORUŃ

Bulletin of Geography. Physical Geography Series, No. 29 (2025): 5–21
http://doi.org/10.12775/bgeo-2025-0007

Assessing seafloor morphological changes of offshore islands based on bathymetry using Sentinel-2 images: a case study in the Truong Sa Islands (Vietnam)

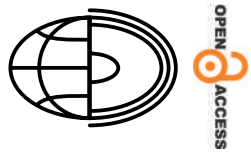

Nhu Hung Nguyen[1], Le Hung Trinh[1]*, Van Phu Le[1], Van Son Nguyen[2]

[1]Le Quy Don Technical University, Institute of Techniques for Special Engineering, 236 Hoang Quoc Viet Street, Hanoi, Vietnam
[2]Sonar Acoustic Technology Department, Naval Technical Institute, Haiphong, Vietnam
*E-mail: trinhlehung@lqdtu.edu.vn
https://orcid.org/0000-0002-2403-063X

Abstract. Assessing seafloor morphological changes plays a crucial role in understanding environmental processes, helping to predict changes in marine ecosystems, protect natural resources, and support sustainable management of marine areas. This study proposes an effective and accurate method for assessing seafloor morphological changes using Sentinel-2 satellite data. The research focuses on analyzing depth and topographic features of offshore islands, with the study area extending 9 km in length and 1.8 km in width, including a semi-enclosed lagoon with depths ranging from 3 to 6 meters. The images were collected at three time points: January 14, 2020; June 5, 2020; and June 15, 2021. Surface reflectance images from the blue and green bands were used to estimate bathymetry. Additionally, the study utilized the Random Forest algorithm on the GEE platform to classify the objects of interest. The results show an increase in the average depth of submarine sand from 2.07 m to 2.17 m, while coral showed a change from 0.96 m to 2.20 m. Coral sand floor and substrate grass also exhibited significant changes in depth, with coral sand floor decreasing from 9.45 m to 6.08 m and substrate grass decreasing from 8.04 m to 6.15 m. Objects such as solid bottom and seagrass maintained stable depths with minor variations. Moreover, field data and tide measurements were used to validate and adjust the bathymetric models, enhancing the accuracy of the estimates.

Key words:
seafloor morphological,
bathymetry,
Sentinel-2,
Truong Sa islands,
Vietnam

Introduction

Seafloor morphology around offshore islands is a vital component in understanding coastal dynamics, marine ecosystems, and the environmental changes occurring in these regions (Pelletier 1986; Roos and Hulscher 2003; Vardar et al. 2024). The bathymetric features of the seafloor, such as depth variations, ridges, valleys and underwater slopes, play an important role in determining ocean currents, sediment transport and the distribution of marine species (Loureiro et al. 2024; Sklar et al. 2024). Consequently, accurate monitoring of seafloor morphological changes is essential for effective marine resource management, environmental conservation and understanding the impact of natural and anthropogenic activities on the marine environment (Andreassen et al. 2008; Linklater et al. 2019).

Traditional bathymetric survey techniques, including ship-based sonar measurements and underwater sensors, have long been the primary methods used to gather data on seafloor topography (Hariram 2024; Xu et al. 2024). However, these methods are often resource-intensive, time-

consuming, and limited in their ability to cover large and remote areas (Zhao et al. 2013). The high cost and complexity of these surveys make it difficult to obtain continuous and wide-scale bathymetric data for many regions, particularly in remote or conflict-prone areas (Traganos et al. 2018).

In recent years, remote sensing technologies, specifically satellite-based sensors, have emerged as a promising solution to overcome these limitations. Among these, the Sentinel-2 mission, a part of the European Space Agency's Copernicus program, offers high-resolution optical imagery with a broad spatial coverage and frequent revisit times (ESA, 2013). While Sentinel-2 satellites are primarily used for land-based observations, their ability to capture detailed surface reflectance data can also be utilized for extracting bathymetric information, particularly in shallow coastal and island regions where the water column is relatively clear (Mateo-Pérez et al. 2020; Mudiyanselage et al. 2022; Almar et al. 2024; Kwon et al. 2024; Richardson et al. 2024).

One common approach for deriving bathymetry from satellite imagery is the Stumpf algorithm, a log-ratio method that relates water depth to the ratio of reflectance in different spectral bands (typically blue and green) (Stumpf et al. 2003). This technique assumes that light attenuation in water varies with depth and uses the relative brightness of pixels to estimate bathymetry in shallow, optically clear waters.

The integration of Sentinel-2 imagery with cloud-based platforms such as Google Earth Engine (GEE) has revolutionized the way remote sensing data are processed and analyzed (GEE 2024). GEE offers a powerful, scalable toolset for processing large datasets and conducting spatial analysis on a global scale. By utilizing this platform, researchers can efficiently analyze large volumes of satellite images to monitor changes in seafloor morphology and bathymetric features over time, providing a cost-effective and timely alternative to traditional survey methods (Traganos et al. 2018; Roca et al. 2022; Merchant et al. 2023).

This study aims to assess the seafloor morphological changes around the Truong Sa Islands using bathymetric data derived from Sentinel-2 imagery. By analyzing changes in depth and topographic features over time, this research seeks to enhance our understanding of the dynamic processes shaping the seafloor in this ecologically important region. Furthermore, this study provides a case study for the application of remote sensing and satellite imagery to seafloor monitoring, demonstrating the potential of Sentinel-2 and Google Earth Engine as tools for sustainable marine resource management and environmental conservation.

Through this research, we aim to fill the gaps in existing bathymetric, seafloor topographic data for the Truong Sa Islands and provide a valuable resource for future studies and policy decisions related to the East Sea. The findings of this study could also be applied to other offshore regions where remote sensing data can be leveraged to monitor seafloor changes, assess environmental impacts and inform conservation strategies on a global scale.

Materials and methodology

Study area

The Truong Sa Islands, located in the East Sea, are known for their complex and diverse underwater topography, which includes coral reefs, shallow sandbanks and deep-sea trenches. The region is of significant ecological and geopolitical importance, hosting rich marine biodiversity and being subject to territorial disputes. Given the dynamic and sensitive nature of the region, monitoring changes in seafloor morphology and bathymetric features is crucial for understanding the effects of natural processes such as tidal shifts and erosion, as well as anthropogenic activities such as dredging, construction and climate change.

The research focuses on offshore islands known for their intricate marine dynamics. The chosen study area extends roughly nine kilometers in length and 1.8 kilometers in width, aligned along a north-east–south-west axis. Within this region lies a semi-enclosed lagoon with depths ranging from three to six meters, bordered by coral reefs and seagrass meadows, both of which are particularly vulnerable to environmental fluctuations.

These islands are ecologically vital and hold significant strategic value for national security. The study area is exposed to a variety of dynamic environmental factors, including wave activity, tidal fluctuations and sediment movement, making it an ideal location for investigating bathymetric changes.

Additionally, the surrounding waters harbor a rich marine ecosystem, and any shifts in bathymetry could have substantial ecological consequences.

Data sources

In this study, Sentinel-2 satellite data accessible through the GEE platform was utilized. Sentinel-2 offers optical imagery with a spatial resolution of ten meters in the visible and near-infrared bands, making it particularly suitable for studying shallow waters (ESA 2024). The data gathered includes surface reflectance values from the Blue (Band 2), Green (Band 3) and Red (Band 4) bands, which are especially valuable for examining water characteristics and estimating depths in coastal and offshore areas.

The data were gathered at specific intervals, with the timing carefully selected to minimize cloud cover, as less cloud cover ensures the most precise surface reflectance measurements. The images were pre-processed in GEE, which included atmospheric correction through the Sen2Cor algorithm, cloud masking, and removal of land and non-water features. These pre-processing steps are essential to ensure that only high-quality data are used for bathymetric estimation.

Along with satellite imagery, tide measurements and field survey bathymetric data were incorporated to validate the bathymetric estimates and adjust for tidal changes. These ground-truth measurements enhance the accuracy of the bathymetric models by providing real-world data for calibration.

Methodology

The methodology employed in this study consists of the following main steps:

Pre-processing Sentinel-2 Imagery:
The Sentinel-2 images were processed to filter out cloud cover and atmospheric interference using GEE's cloud masking functions. Areas that were not water bodies were excluded by applying specific threshold values for the study area: Green band reflectance (ρGREEN > 0.01), Red band reflectance (ρRED < 0.1), and Near-Infrared band reflectance (ρNIR < 0.03). This procedure ensures that only data from water bodies are used for depth estimation, reducing the influence of noise caused by land or cloud cover.

Bathymetric estimation:

The next step is to apply the Normalized Difference Water Index (NDWI) to enhance the contrast between water and land features in order to extract the water surface. The NDWI index was calculated according to the following formula (McFeeters 1996):

$$NDWI = \frac{\rho_{GREEN} - \rho_{NIR}}{\rho_{GREEN} + \rho_{NIR}} \quad (1)$$

where ρGREEN, ρNIR – reflectance values in the GREEN (Band 3) and NIR (Band 8) bands of the Sentinel-2 multispectral image. The reflectance values were then used to calculate the remote sensing reflectance (Rrs) using established algorithms. The Stumpf algorithm, which correlates water depth with the attenuation of blue and green light, was used for estimating water depth (Stumpf et al. 2003). This algorithm is widely used for deriving bathymetry from multispectral satellite imagery due to its ability to account for varying water clarity and bottom types (Hung and Phu 2023).

Additionally, the concentration of chlorophyll-a (Chl-a) was incorporated into the model to refine the depth estimates (Li et al. 2019). Chlorophyll-a concentrations affect the optical properties of water and can influence the accuracy of depth retrieval. In this study, a fixed Chl-a value of 0.5 mg/m^3 was used based on previous research in similar regions (Li et al. 2021). The depth estimation parameters (m and n) of the Stumpf algorithm are respectively calculated according to formulas (2) and (3):

$$m = a * e^{(0.957 * Chl-a)} \quad (2)$$

$$n = b * e^{(0.957 * Chl-a)} \quad (3)$$

Finally, the study estimates water depth by quantifying the different attenuation levels between the blue and green image band (Stumpf et al. 2003):

$$Depth = m \frac{\ln(1000 * r_{rs} blue)}{\ln(1000 * r_{rs} green)} + n \quad (4)$$

where a and b are the optimal parameters. To determine the values of a and b, the authors use field measurement data combined with a linear regression algorithm. The parameters m and n will be calculated after the linear regression process.

Tidal and calibration adjustments:
After estimating the depth, tidal data from three time periods were used to adjust the bathymetric values to a consistent tidal reference. The tidal difference between times is calculated. This correction for variation ensures that the bathymetric changes reflect actual seafloor movements rather than tidal fluctuations. In-situ bathymetric measurements collected during field surveys were also used to calibrate the bathymetric estimates, improving the accuracy and reliability of the results.

Change detection:
The image difference has been used to detect depth changes between the time. By deducting depth values with the same pixel position, the discovery map has been created to visualize the areas where the depth variations occur.

Object classification:
In this study, the Random Forest (RF) algorithm was used on the Google Earth Engine (GEE) platform to classify the study area into seven distinct objects of interest including submarine sand, coral, solid bottom, seagrass, substrate grass, land and coral sand floor. The algorithm was trained using labeled samples representing different object features (Breiman 2001). These features were distinguished based on reflectance values from Sentinel-2 bands. By leveraging the computational power of GEE, the RF classifier processed a large number of pixels, effectively distinguishing the seven objects with high accuracy. The resulting classification provides valuable insights into the distribution and spatial patterns of seafloor features, contributing to more accurate terrain variability analysis.

Results and discussion

Sentinel-2 data were collected at three specific time points: January 14, 2020; June 5, 2020; and June 15, 2021. These time points were carefully chosen based on cloud cover levels, as less cloud cover ensures higher accuracy in measuring surface reflectance. With minimal cloud cover, satellite sensors can capture clear images of the water surface, ensuring that the reflected data truly reflect underwater conditions without being affected by clouds. Choosing these times helps enhance the accuracy and reliability of the data, ensuring that the images obtained reflect the actual conditions of the study area. Additionally, the tidal difference between January 14, 2020 (0.4 m) and June 5, 2020 (1.6 m) was 1.4 m, and between June 5, 2020, and June 15, 2021 (1.8 m) was 0.4 m.

Figures 1–3 show Sentinel-2 satellite images and derived depth map of the study area on, respectively, January 14, 2020; June 5, 2020; and June 15, 2021. The Sentinel-2 images are displayed in natural

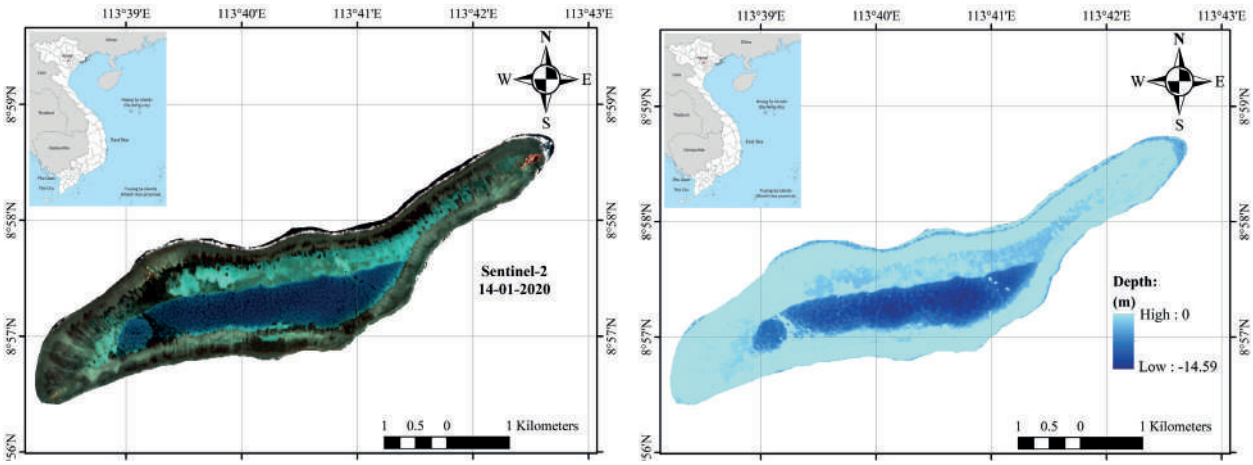

Fig. 1. Sentinel-2 image and derived depth map of the study area on January 14, 2020

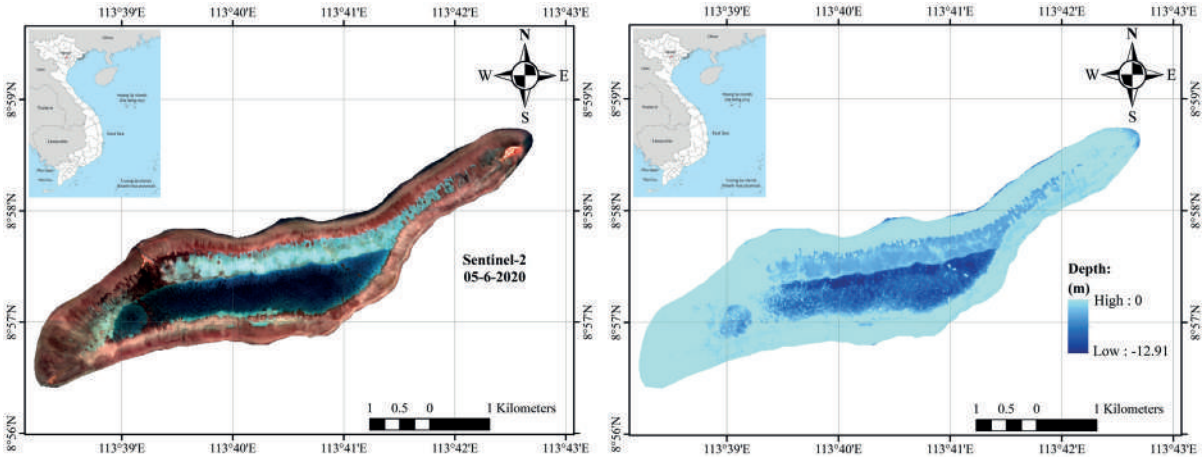

Fig. 2. Sentinel-2 image and derived depth map of the study area on June 5, 2020

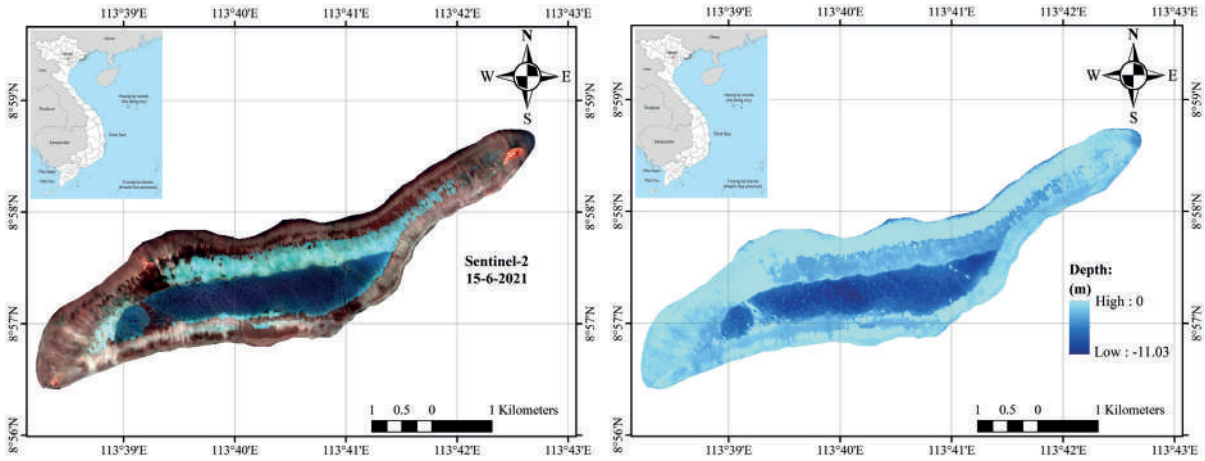

Fig. 3. Sentinel-2 image and derived depth map of the study area on June 15, 2021

color composite (Red-Green-Blue). In addition, bathymetric maps obtained from Sentinel-2 satellite images are presented. Overall, the depths ranged from 0 m to less than 15 m. Notably, the depth tends to increase toward the center of the basin in the study area. Moreover, the distribution of depth values clearly reflects the characteristic terrain of the area, with shallow depths near the edges and greater depths in the central region. This is significant for analyzing the topography and evaluating the resource potential of the basin, as well as providing input data for prediction models related to resources and the environment.

Figure 4 illustrates the distribution of field measurement points. A total of 253 measurement points were recorded, with depths ranging from 0 m to 1.1 m.

Figure 5 illustrates the linear regression results between depth determined from satellite images and field measurement depth on January 14, 2020. The x-axis represents depth from satellite images, while the y-axis represents field measurement depth. The linear regression equation $y = 0.901x + 0.053$ with $R^2 = 0.889$ shows a strong, near-linear relationship between the two variables, with 88.9% of the variation in field measurements explained by satellite image data. The data points are represented by two different colors: blue (diamond) for depth from satellite images and orange (square) for field measurement depth.

Figure 6 presents the linear regression results between depth determined from satellite images and field measurement depth on June 5, 2020. The resulting regression equation $y = 0.976x + 0.056$ and $R^2 = 0.948$ show a very strong correlation between

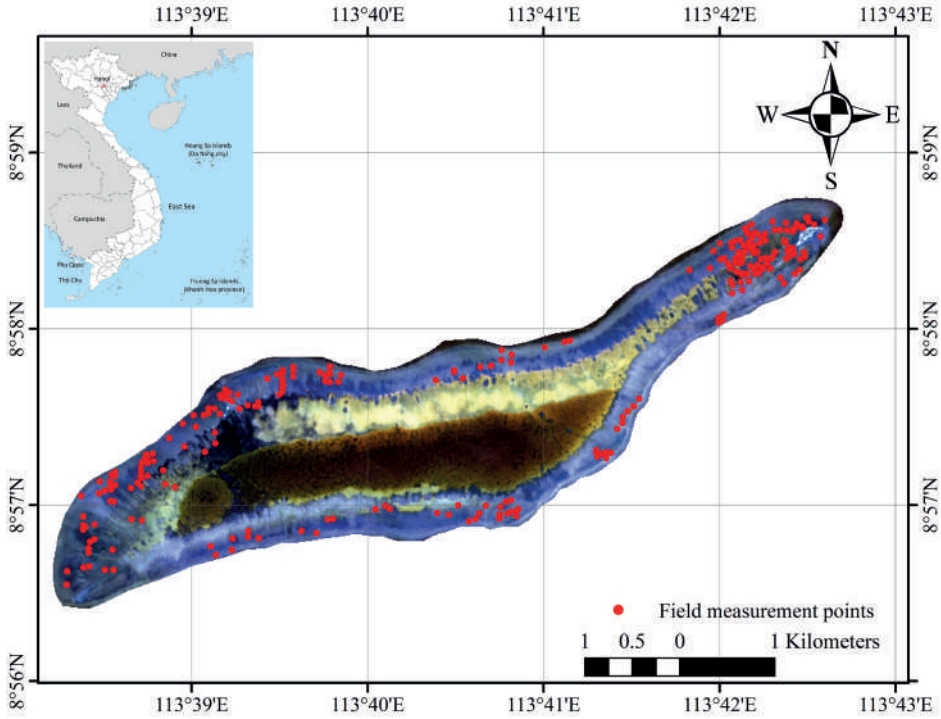

Fig. 4. Distribution of field measurement points

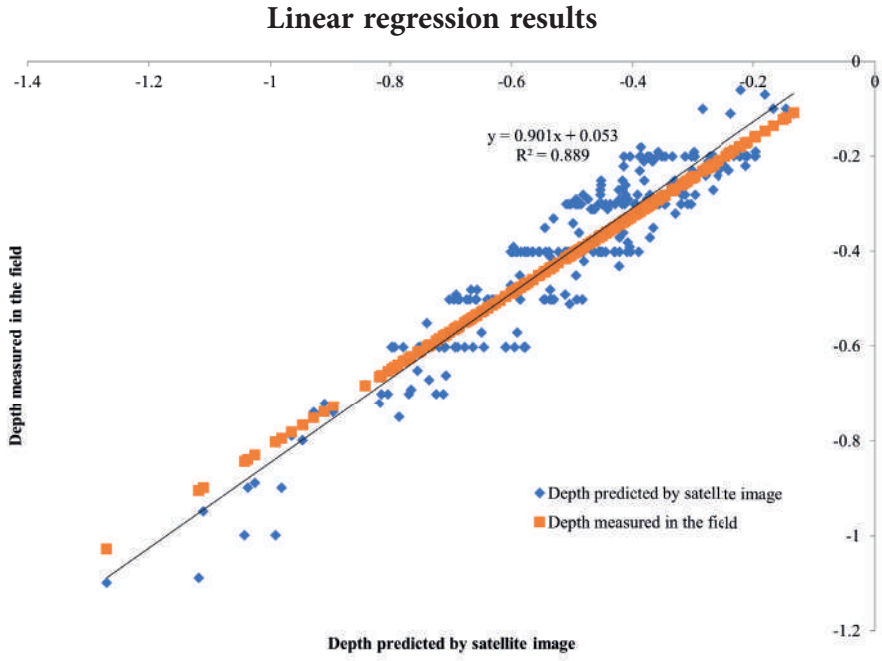

Fig. 5. Comparison of depth determined from Sentinel-2 image on January 14, 2020 with field measurement results

the two variables, with 94.8% of the variation in field measurements explained by satellite image data. The data points, colored blue (depth from satellite images) and orange (field measurement depth), are tightly clustered around the regression line, indicating low error and good fit.

Similarly, Figure 7 shows the linear regression results between depth determined from satellite

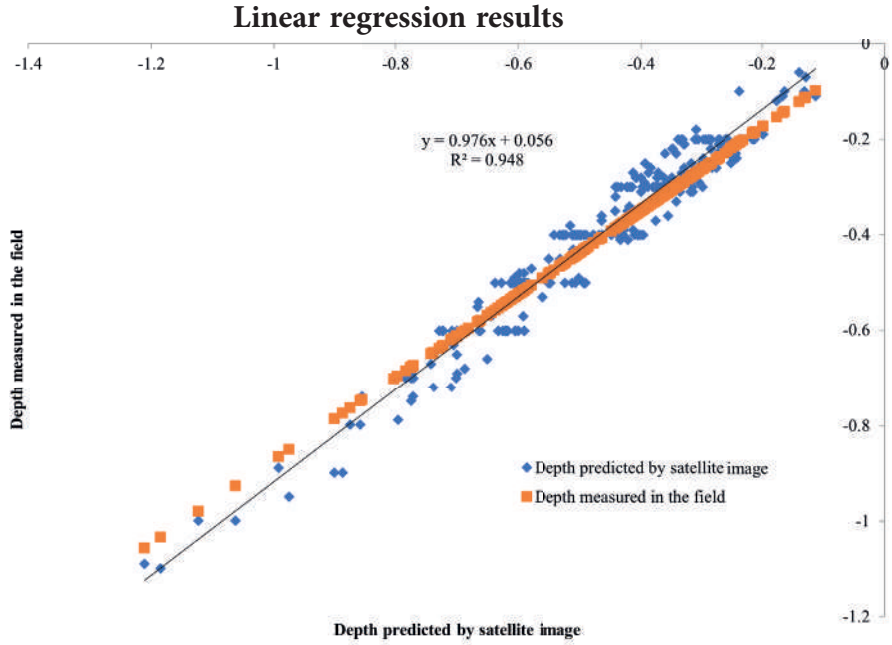

Fig. 6. Comparison of depth determined from Sentinel-2 image on June 5, 2020 with field measurement results

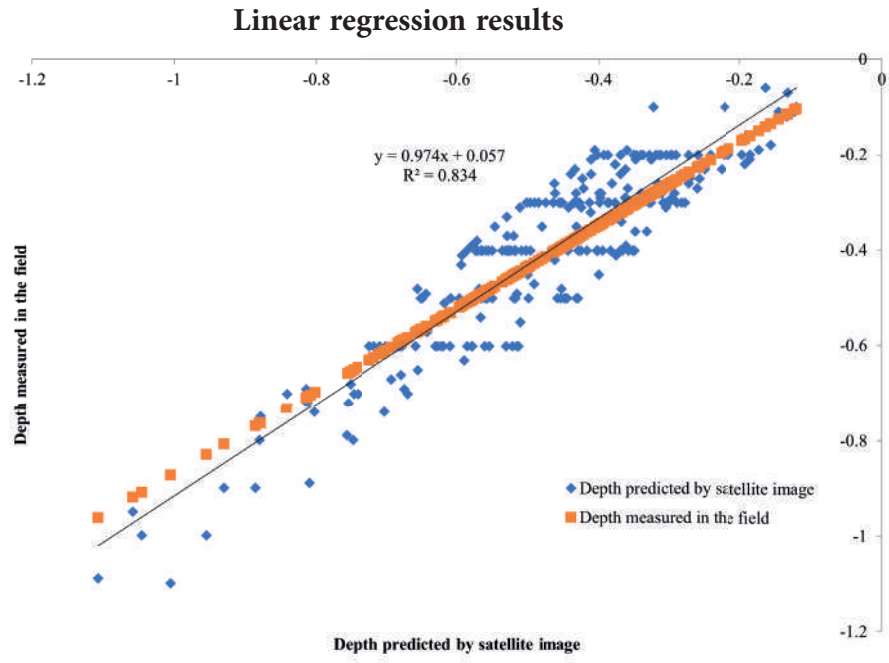

Fig. 7. Comparison of depth determined from Sentinel-2 image on June 15, 2021 with field measurement results

images and field measurement depth on June 15, 2021, with slightly lower results. The regression equation $y = 0.974x + 0.057$ with $R^2 = 0.834$ indicates that 83.4% of the variation in field measurements can be explained by satellite image data. Although there is still a good correlation, the data points are more scattered around the regression line, indicating higher errors compared to the previous two results.

This may be due to factors such as noise or errors during data collection. However, the results still show the feasibility of using satellite images for depth determination, despite lower accuracy.

The regression line closely follows the data points, indicating that the satellite image depth determination method is highly accurate compared to field measurements. However, some points deviating from the regression line may be due to noise or measurement errors. This suggests the potential application of satellite images to determine depth, helping reduce costs and time compared to traditional field measurements.

Additionally, the RMSE (Root Mean Square Error) results are 0.066 m, 0.048 m, and 0.079 m, showing the average deviation between predicted and actual values in the study of depth variations around the study area. These relatively low values reflect that the model is highly accurate in estimating coastal depths. Moreover, this result proves that the method using satellite images to determine depth is highly accurate and reliable, suitable for application in practical research.

Figure 8 illustrates the change in water depth in the study area from January 14, 2020, to June 5, 2020. The map uses a color scale to represent depth changes, ranging from –9.92 meters to 9.05 meters. Deeper water areas are shown in blue and purple, mainly concentrated in the central basin, indicating erosion or subsidence. In contrast, shallower areas, shown in yellow and brown, reflect sediment deposition. The map shows significant spatial changes, with uneven depth variations across the area.

Similarly, Figure 9 records the depth changes in the study area from June 5, 2020, to June 15, 2021. The depths ranged from –7.05 meters to 8.34 meters, with deeper areas shown in blue and purple, while yellow to brown shades represent shallower areas. The central basin shows a significant increase in depth, possibly due to erosion, while areas with brown shades clearly indicate sediment deposition, which leads to water being shallower.

Figures 10 and 11 show the locations of cross-sections and the corresponding depth variation values for each cross-section. Figure 11 shows the central area of the study area experiencing the most significant depth variation. This area, characterized by great depths, is more susceptible to changes due to both geological dynamics and environmental factors. Geological changes, such as tectonic movements or sediment shifts, may significantly alter the bottom topography, while the development and expansion of vegetation in the water environment can also

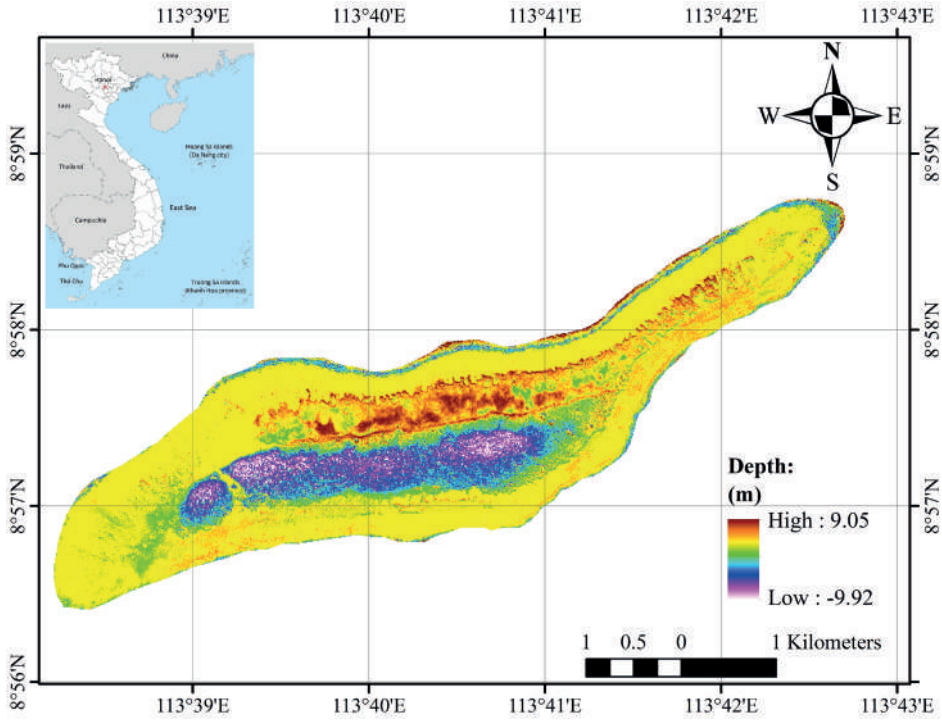

Fig. 8. Depth change map in the study area from January 14, 2020 to June 5, 2020

Citation: Bulletin of Geography. Physical Geography Series 2025, 29, http://doi.org/10.12775/bgeo-2025-0007

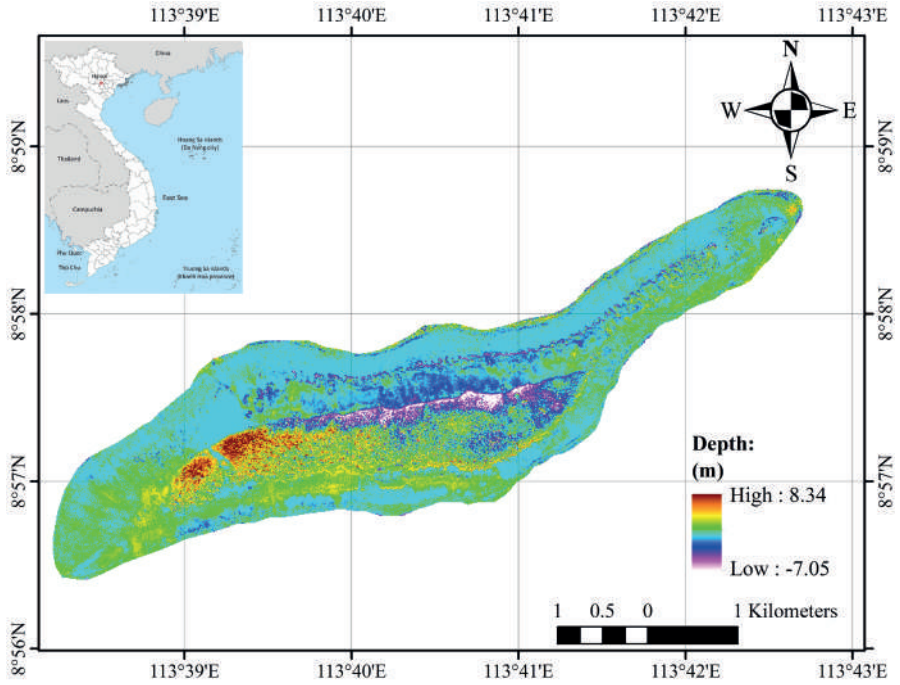

Fig. 9. Depth change map in the study area from June 5, 2020 to June 15, 2021

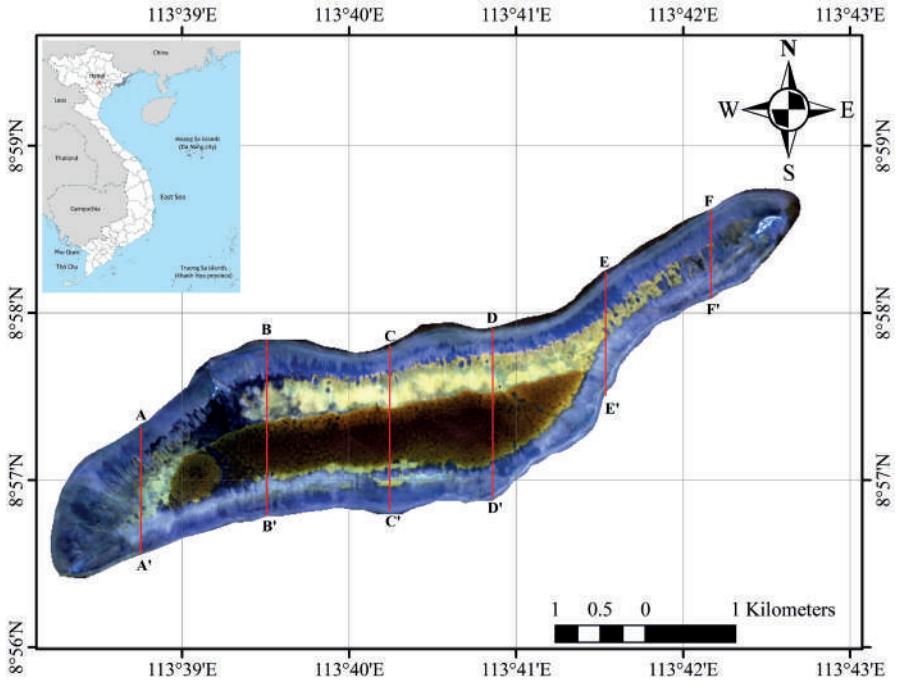

Fig. 10. Depth change map in the study area from June 5, 2020 to June 15, 2021

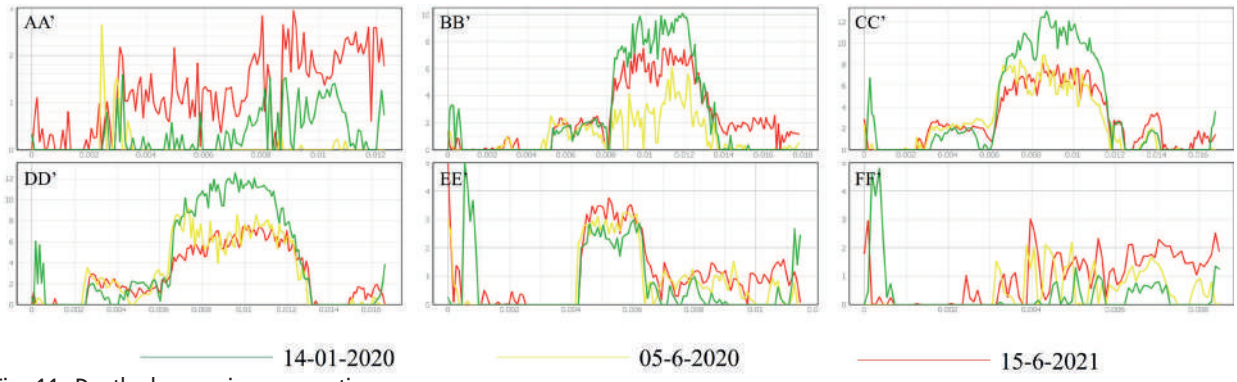

Fig. 11. Depth changes in cross-sections

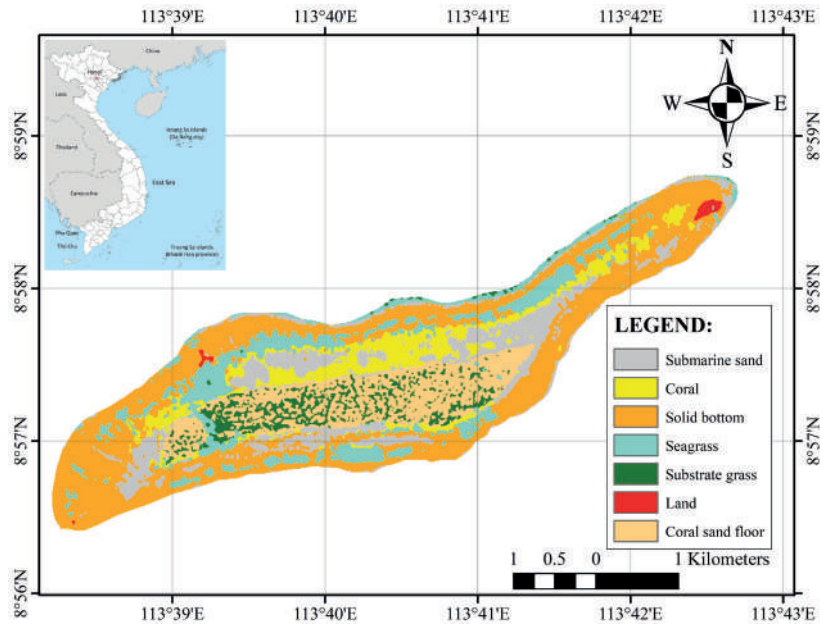

Fig. 12. Classification results of Sentinel-2 image in the study area on January 14, 2020

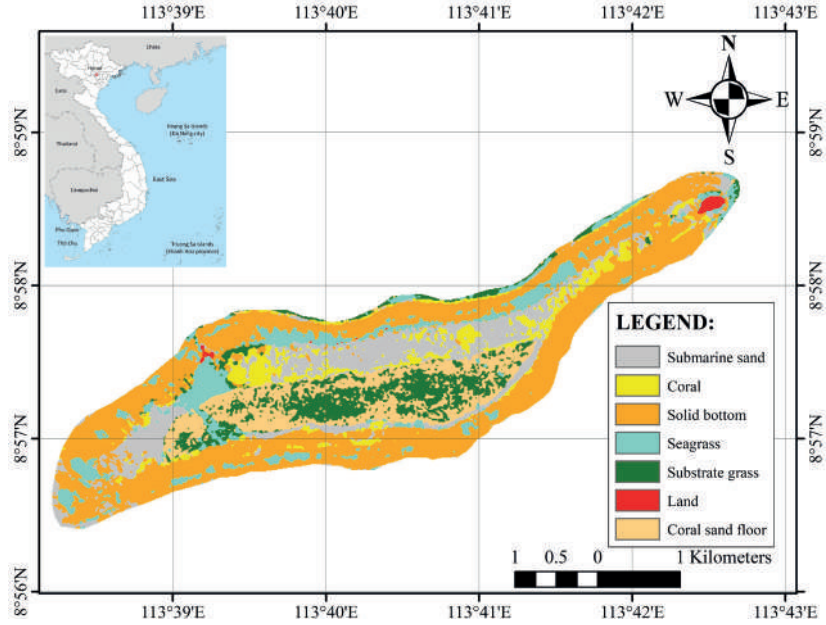

Fig. 13. Classification results of Sentinel-2 image in the study area on June 5, 2020

Citation: Bulletin of Geography. Physical Geography Series 2025, 29, http://doi.org/10.12775/bgeo-2025-0007

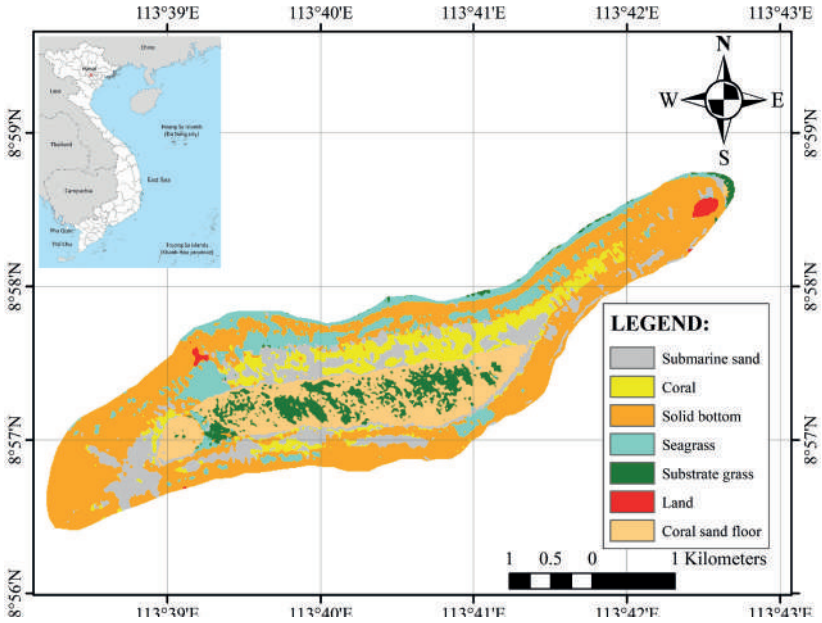

Fig. 14. Classification results of Sentinel-2 image in the study area on June 15, 2021

Table 1. Area of classified objects in the study area from Sentinel-2 images

Date	January 14, 2020		June 5, 2020		June 15, 2021	
Class	ha	%	ha	%	ha	%
Submarine sand	189.06	14.98	200.73	15.90	183.18	14.51
Coral	133.57	10.58	97.36	7.71	120.25	9.53
Solid bottom	511.63	40.53	543.77	43.07	548.43	43.44
Seagrass	173.05	13.71	139.04	11.01	138.82	11.00
Substrate grass	68.86	5.45	127.24	10.08	78.71	6.23
Land	6.25	0.50	6.32	0.50	7.77	0.62
Coral sand floor	179.97	14.26	147.93	11.72	185.23	14.67

contribute to these changes over time. Therefore, this central area is more vulnerable and needs to be monitored for natural and environmental changes.

These variations show the dynamic interactions between natural processes, including tidal forces, currents and wave activity, which have reshaped the underwater topography. The sharp contrasts between deep and shallow regions highlight the ongoing sediment transport and morphological changes in the area. These findings emphasize the importance of continuous observation to better understand and manage coastal erosion and sediment deposition, ensuring sustainable development for affected offshore areas.

Figures 12–15 show the classification results from Sentinel-2 images of the study area on January 14, 2020, June 5, 2020, and June 15, 2021. The classification accuracy using the Random Forest algorithm exceeded 90%, ensuring the reliability of the results. Table 1 shows the area (ha) and percentage (%) of classified objects in the study area. This data provides detailed information about the area changes of different objects over the study time points, reflecting environmental fluctuations in the region as follows:

Submarine sand: The area of submarine sand fluctuated slightly across the time points, with 189.06 ha (14.98%) on January 14, 2020, increasing to 200.73 ha (15.90%) on June 5, 2020, and decreasing to 183.18 ha (14.51%) on June 15, 2021. This change reflects the effects of erosion and sand deposition due to factors such as tides, waves or coastal currents.

Coral: The coral area declined from 133.57 ha (10.58%) on January 14, 2020, to 97.36 ha (7.71%) on June 5, 2020, but then slightly increased to 120.25 ha (9.53%) on June 15, 2021. The reduction in 2020 may be due to environmental impacts such as climate change or human activities, while the recovery in 2021 may be the result of more favorable environmental conditions.

Solid bottom: The solid bottom covered the largest area in the study area and showed a slight increase over time. On January 14, 2020, the area was 511.63 ha (40.53%), increasing to 543.77 ha (43.07%) on June 5, 2020, and reaching 548.43 ha (43.44%) on June 15, 2021. This suggests the stability or development of solid bottom layers, possibly due to sediment deposition or stable underwater conditions.

Seagrass: The seagrass area significantly decreased over time. On January 14, 2020, the area was 173.05 ha (13.71%), but by June 5, 2020, it had decreased to 139.04 ha (11.01%) and further decreased to 138.82 ha (11.00%) on June 15, 2021. This trend may indicate the degradation of the seagrass ecosystem, potentially due to human activities or changes in water quality.

Substrate grass: Substrate grass area increased significantly from 68.86 ha (5.45%) on January 14, 2020, to 127.24 ha (10.08%) on June 5, 2020, but then decreased slightly to 78.71 ha (6.23%) on June 15, 2021. This fluctuation may relate to environmental factors or temporary growth of this type of underwater vegetation.

Land: The land area in the study area showed very slight changes, fluctuating from 6.25 ha (0.50%) on January 14, 2020, to 6.32 ha (0.50%) on June 5, 2020, and increasing to 7.77 ha (0.62%) on June 15, 2021. This suggests the stability of the land area within the study region.

Coral sand floor: The coral sand floor area decreased from 179.97 ha (14.26%) on January 14,

Table 2. Minimum, maximum, average values and standard deviation by depth of classified objects on January 14, 2020

Object	Minimum	Maximum	Average	Standard deviation
Submarine sand	0.02	3.53	2.07	0.56
Coral	0.06	6.88	0.96	1.02
Solid bottom	0.00	1.15	0.17	0.09
Seagrass	0.00	5.12	0.17	0.74
Substrate grass	3.25	14.52	8.04	3.00
Coral sand floor	2.71	14.59	9.45	2.22

Table 3. Minimum, maximum, average values and standard deviation by depth of classified objects on June 5, 2020

Object	Minimum	Maximum	Average	Standard deviation
Submarine sand	0.01	4.06	1.73	1.14
Coral	0.10	8.60	1.58	1.29
Solid bottom	0.00	1.50	0.16	0.06
Seagrass	0.01	5.85	0.21	0.69
Substrate grass	3.53	12.22	6.76	2.76
Coral sand floor	3.14	12.91	7.06	2.65

Table 4. Minimum, maximum, average values and standard deviation by depth of classified objects on June 15, 2021

Object	Minimum	Maximum	Average	Standard deviation
Submarine sand	0.01	3.41	2.17	1.01
Coral	0.10	6.23	2.20	0.64
Solid bottom	0.00	1.24	0.22	0.05
Seagrass	0.00	4.51	0.39	0.85
Substrate grass	2.59	11.03	6.15	1.81
Coral sand floor	3.41	10.36	6.08	1.40

Citation: Bulletin of Geography. Physical Geography Series 2025, 29, http://doi.org/10.12775/bgeo-2025-0007

2020, to 147.93 ha (11.72%) on June 5, 2020, and then increased to 185.23 ha (14.67%) on June 15, 2021. This fluctuation may reflect the movement and accumulation of sediment in the seabed.

June 15, 2021. This data reflects changes in depth and the distribution of seafloor topographic features over time, offering important insights into the environmental dynamics of the region.

For submarine sand, the average value increased from 2.07 m on January 14, 2020, to 2.17 m on June 15, 2021, although there was a slight decrease on June 5, 2020 (1.73 m). The standard deviation also gradually increased over time, from 0.56 to 1.01, indicating a rise in the variability of sand depth. This change could be attributed to the effects of waves, currents or sediment deposition.

Coral showed a trend of decreasing maximum values (from 6.88 m in 2020 to 6.23 m in 2021), while the average value increased from 0.96 m to 2.20 m. In addition, the standard deviation decreased from 1.02 in 2020 to 0.64 in 2021, reflecting more uniform depth distribution over time, possibly due to the stability of coral or degradation in some areas.

The solid bottom remained stable with a low average value (0.17 m in 2020, 0.16 m in 2020, and 0.22 m in 2021) and a very small standard deviation (ranging from 0.05 to 0.09). This indicates that the solid bottom terrain experienced minimal changes throughout the study period.

Seagrass exhibited a significant decrease in average value from 0.17 m on January 14, 2020, to 0.39 m on June 15, 2021. However, the standard

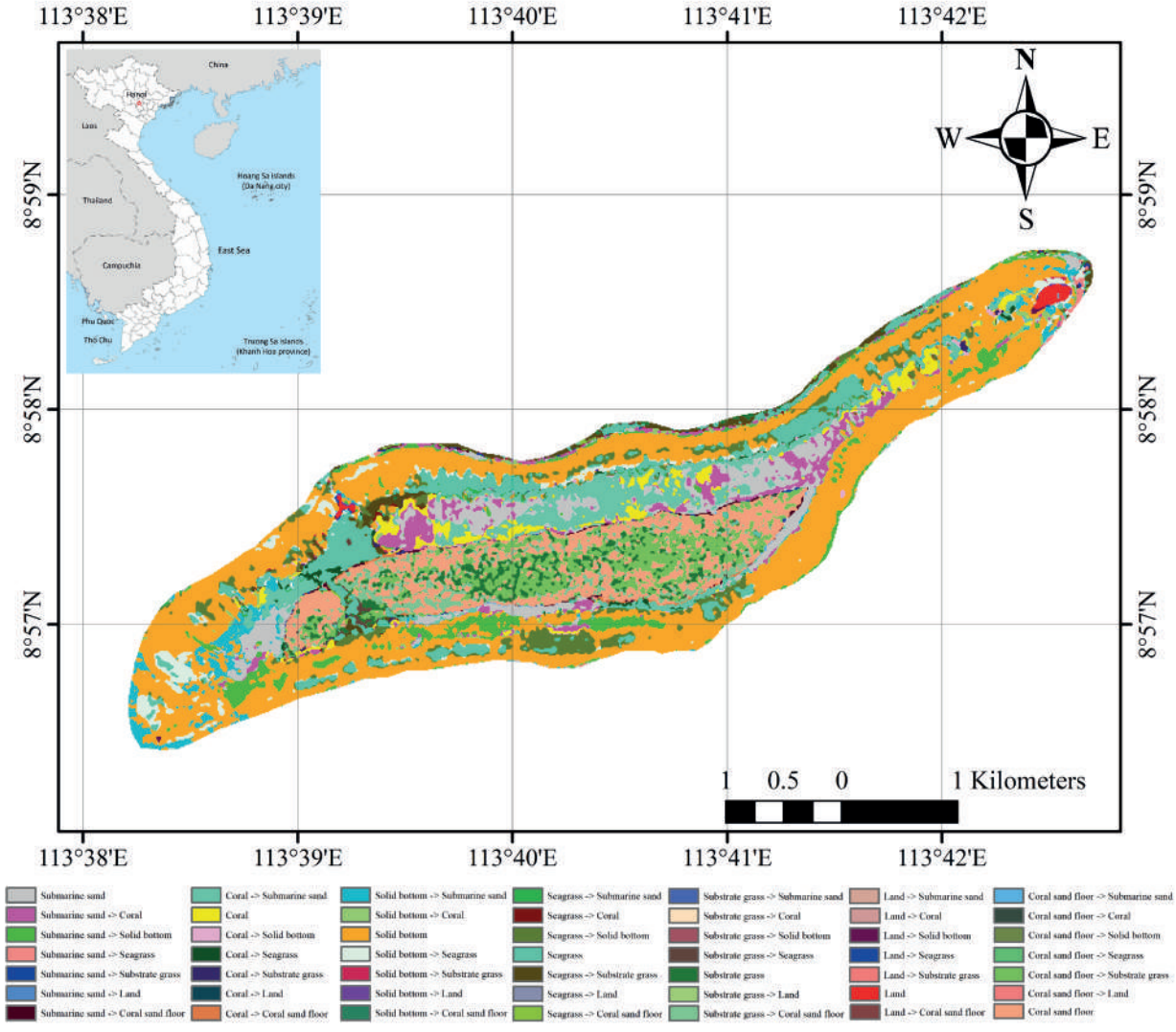

Fig. 15. Geomorphological change map of the study area from January 14, 2020 to June 5, 2020

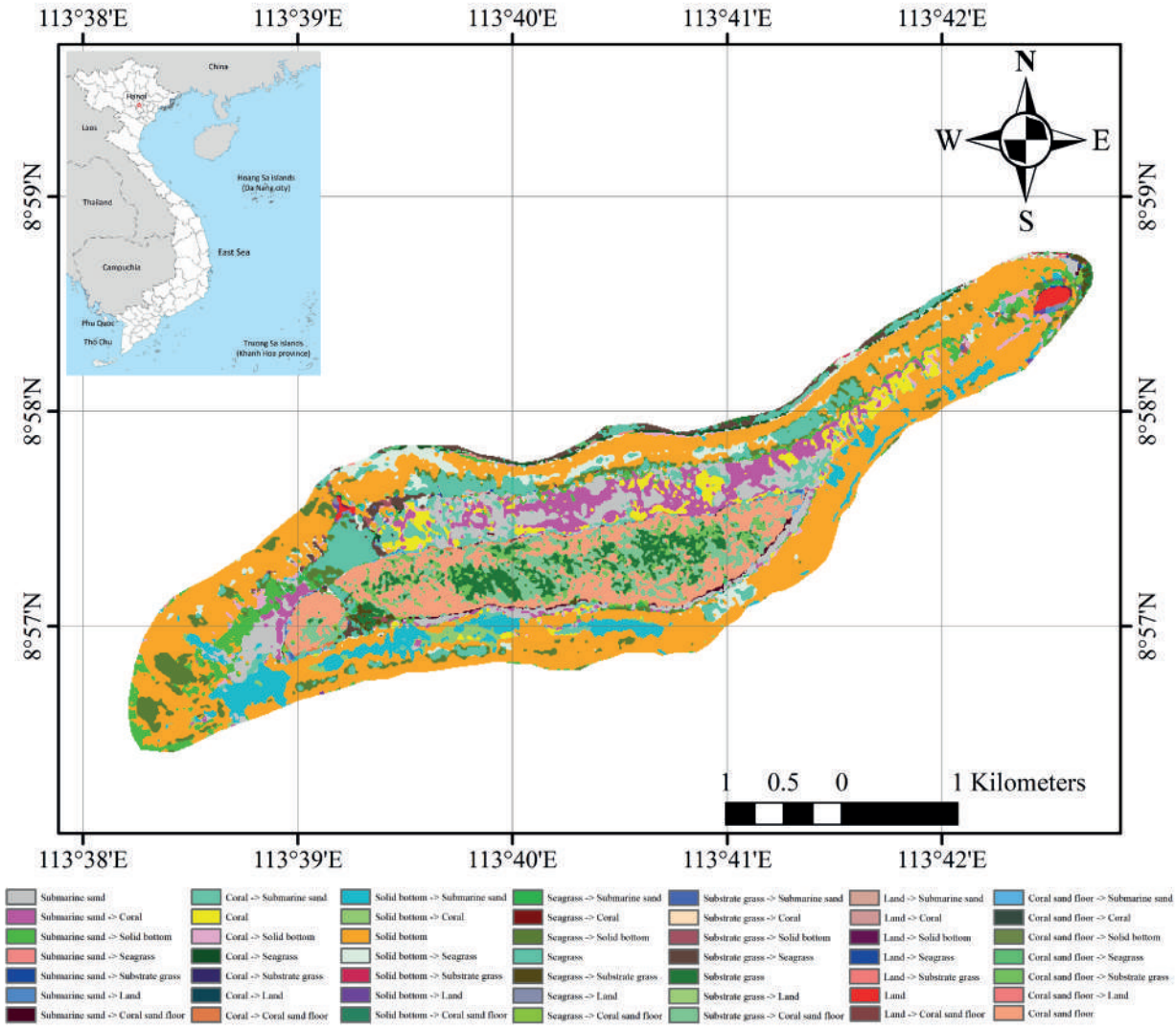

Fig. 16. Geomorphological change map of the study area from June 5, 2020 to June 15, 2021

deviation slightly increased from 0.74 to 0.85, reflecting changes in the depth distribution of seagrass, which may be related to a decrease in biomass or changing environmental conditions.

For substrate grass, the average value decreased from 8.04 m in 2020 to 6.15 m in 2021, although the minimum and maximum values remained relatively unchanged. The standard deviation decreased from 3.00 in 2020 to 1.81 in 2021, indicating that the variability of substrate grass depth decreased over time, possibly due to sediment deposition or the spread of underwater vegetation.

Finally, coral sand floor showed a decrease in the average value from 9.45 m in 2020 to 6.08 m in 2021, accompanied by a reduction in standard deviation from 2.22 to 1.40. This suggests changes in the distribution of coral sand sediments, likely influenced by wave action or biological activities on the seafloor. Figures 15, 16, and 17, respectively, present the seafloor morphological change maps of the study area across different time periods.

One of the challenges encountered in depth determination is the presence of clouds, which limits the number of images that can be used. However, the cloud-based processing capability of GEE has enabled efficient handling of large datasets, generating reliable depth maps despite these limitations.

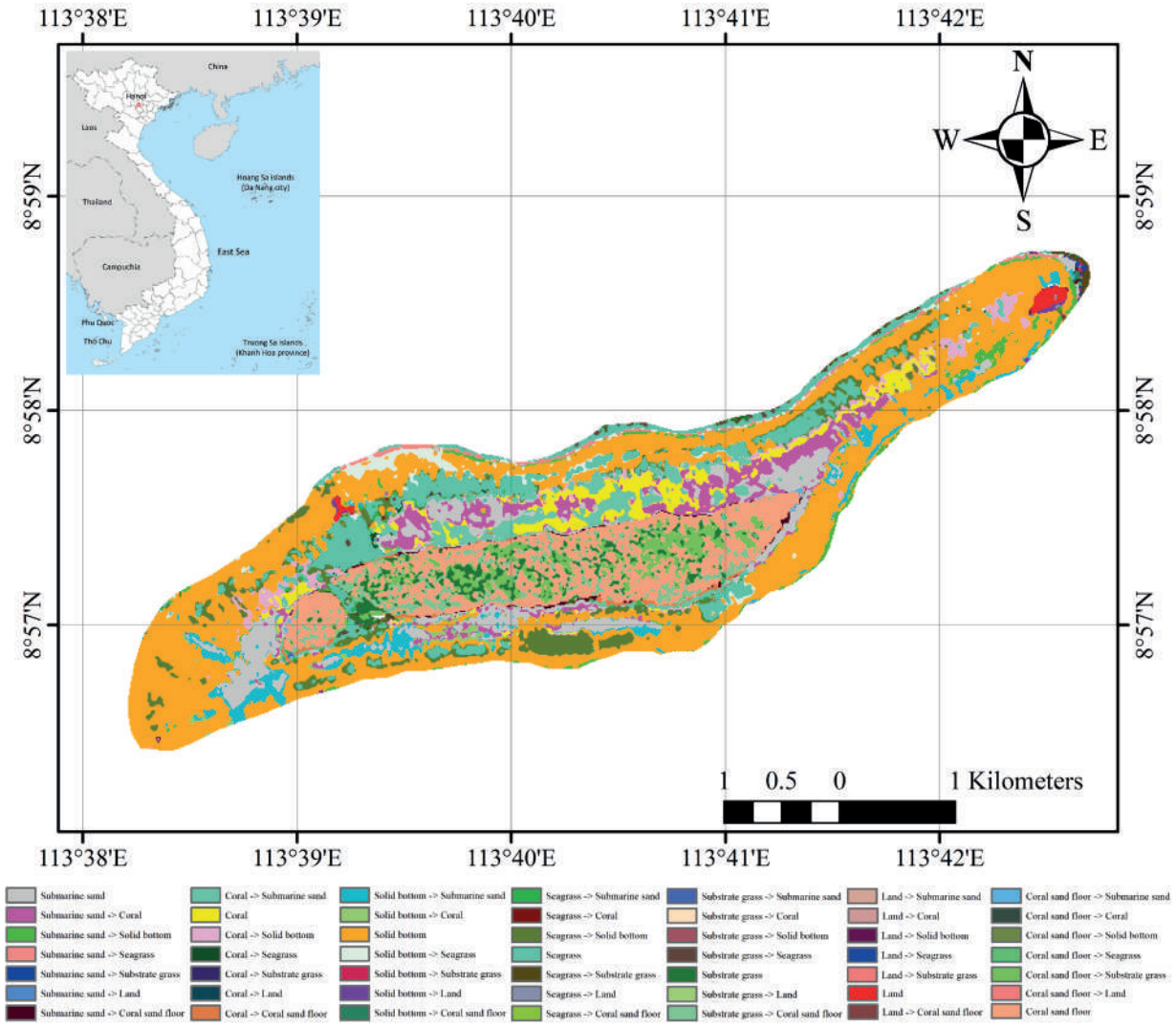

Fig. 17. Geomorphological change map of the study area from January 14, 2020 to June 15, 2021

Conclusion

This study applied a method using Sentinel-2 satellite imagery combined with the Random Forest algorithm on the GEE platform to analyze and assess the seafloor morphological changes of offshore in the Truong Sa islands. The results from the classification model revealed significant variations in depth and the distribution of seafloor objects, including submarine sand, coral, solid bottom, seagrass, substrate grass and coral sand floor. Submarine sand and coral showed notable changes in depth, with an increase in the average depth of submarine sand and significant changes in coral areas. Coral sand floor and substrate grass also exhibited changes, with a decrease in depth in these areas, reflecting environmental impacts and ecological factors. The bathymetric models were adjusted and validated through field data and tide measurements, enhancing the accuracy of the depth estimates. This method not only provides valuable insights into seafloor topography changes but also offers a useful tool for monitoring and managing marine resources, especially in the context of climate change and human impacts on the marine environment. The use of satellite data helps reduce costs and time compared to traditional tidal survey methods, while providing accurate and timely information for research and marine conservation strategies. However, cloud cover limits the usability of satellite images. Future studies should explore

higher-resolution imagery and advanced methods to improve bathymetric accuracy.

Disclosure statement

No potential conflict of interest was reported by the authors

Author contributions

Study design: NHN, LHT; data collection: NHN, VPL; statistical analysis: LHT, VPL; result interpretation: LHT, VSN; manuscript preparation: NHV, VPL; literature review: NHN, LHT, VSN

References

ALMAR R, BERGSMA EW, THOUMYRE G, SOLANGE LC, LOYER S, ARTIGUES S and LIFERMANN A, 2024, Satellite-derived bathymetry from correlation of Sentinel-2 spectral bands to derive wave kinematics: Qualification of Sentinel-2 S2Shores estimates with hydrographic standards. *Coastal Engineering*, 189: 104458. DOI: https://doi.org/10.1016/j.coastaleng.2024.104458.

ANDREASSEN K, LABERG JS and VORREN TO, 2008, Seafloor geomorphology of the SW Barents Sea and its glaci-dynamic implications. *Geomorphology* 97(1-2): 157-177. DOI: https://doi.org/10.1016/j.geomorph.2007.02.050.

BREIMAN L, 2001, Random Forests. *Machine Learning* 45: 5–32. DOI: https://doi.org/10.1023/A:1010933404324.

EUROPEAN SPACE AGENCY, 2024, Available at: https://sentinel.esa.int/web/sentinel/copernicus/sentinel-2 (Accessed 20 December 2024).

GOOGLE EARTH ENGINE. Harmonized Sentinel-2 MSI: MultiSpectral Instrument, Level-2A. Available at: https://developers.google.com/earth-engine/datasets/catalog/COPERNICUS_S2_SR_HARMONIZED (Accessed 31 December 2024)..

HARIRAM V, 2024, *Bathymetry, the future potential of ocean mapping, and the seafloor revolution*. Available at SSRN 4977191.

KWON JY, SHIN HK, KIM DH, LEE HG, BOUK JK, KIM JH and KIM TH, 2024, Estimation of shallow bathymetry using Sentinel-2 satellite data and random forest machine learning: a case study for Cheonsuman, Hallim, and Samcheok Coastal Seas. *Journal of Applied Remote Sensing* 18(1): 014522-014522. DOI: https://doi.org/10.1117/1.JRS.18.014522.

LI J, KNAPP DE, SCHILL SR, ROELFSEMA C, PHINN S, SILMAN M, MASCARO J and ASNER GP, 2019, Adaptive Bathymetry Estimation for Shallow Coastal Waters Using Planet Dove Satellites. *Journal of Applied Remote Sensing* 18(1): 014522-014522. DOI: https://doi.org/10.1016/j.rse.2019.111302.

LI J, KNAPP DE, LYONS M, ROELFSEMA C, PHINN S, SCHILL SR and ASNER GP, 2021, Automated Global Shallow Water Bathymetry Mapping Using Google Earth Engine. *Remote Sensing* 13(8): 1469. DOI: https://doi.org/10.3390/rs13081469.

LINKLATER M, INGLETON TC, KINSELA MA, MORRIS BD, ALLEN KM, SUTHERLAND MD and HANSLOW DJ, 2019, Techniques for classifying seabed morphology and composition on a subtropical-temperate continental shelf. *Geosciences* 9(3): 141. DOI: https://doi.org/10.3390/geosciences9030141.

LOUREIRO G, DIAS A, ALMEIDA J, MARTINS A, HONG S and SILVA E, 2024, A Survey of Seafloor Characterization and Mapping Techniques. *Remote Sensing* 16(7): 1163. DOI: https://doi.org/10.3390/rs16071163.

MATEO-PÉREZ V, CORRAL-BOBADILLA M, ORTEGA-FERNÁNDEZ F and VERGARA-GONZÁLEZ EP, 2020, Port bathymetry mapping using support vector machine technique and sentinel-2 satellite imagery. *Remote sensing* 12(13): 2069. DOI: https://doi.org/10.3390/rs12132069.

MCFEETERS SK, 1996, The use of the Normalized Difference Water Index (NDWI) in the delineation of open water features. *International Journal of Remote Sensing* 17(7): 1425–1432. DOI: https://doi.org/10.1080/01431169608948714.

MERCHANT MA, 2023, Modelling inland Arctic bathymetry from space using cloud-based machine learning and Sentinel-2. *Advances in Space Research* 72(10): 4256-4271.

MUDIYANSELAGE SSJD, ABD-ELRAHMAN A, WILKINSON B and LECOURS V, 2022, Satellite-

derived bathymetry using machine learning and optimal Sentinel-2 imagery in South-West Florida coastal waters. *GIScience & Remote Sensing* 59(1): 1143-1158. DOI: https://doi.org/10.1080/15481603.2022.2100597.

NGUYEN NH and PHU LV, 2023, Bathymetric mapping of Co To island area, Quang Ninh province using sentinel-2 and landsat 8 images. *Journal of Science and Technique-Section on Special Construction Engineering* 6(01). DOI: https://doi.org/10.56651/lqdtu.jst.v6.n01.663.sce.

PELLETIER BR, 1986, Seafloor morphology and sediments. *Canadian Inland Seas* 44: 143-162.

RICHARDSON G, FOREMAN N, KNUDBY A, WU Y and LIN Y, 2024, Global deep learning model for delineation of optically shallow and optically deep water in Sentinel-2 imagery. *Remote Sensing of Environment* 311: 114302. DOI: https://doi.org/10.1016/j.rse.2024.114302.

ROCA M, NAVARRO G, GARCÍA-SANABRIA J and CABALLERO I, 2022, Monitoring sand spit variability using Sentinel-2 and Google Earth Engine in a Mediterranean estuary. *Remote Sensing* 14(10): 2345. DOI: https://doi.org/10.3390/rs14102345.

ROOS PC and HULSCHER SJ, 2003, Large-scale seabed dynamics in offshore morphology: Modeling human intervention. *Reviews of geophysics* 41(2): 1-21. DOI: https://doi.org/10.1029/2002RG000120.

SKLAR E, BUSHUEV E, MISIUK B, LABBÉ-MORISSETTE G and BROWN CJ, 2024, Seafloor morphology and substrate mapping in the Gulf of St Lawrence, Canada, using machine learning approaches. *Frontiers in Marine Science* 11: 1306396.

STUMPF RP, HOLDERIED K and SINCLAIR M, 2003, Determination of Water Depth with High-Resolution Satellite Imagery Over Variable Bottom Types. *Limnology and Oceanography* 48(1): 547–556.

THE EUROPEAN SPACE AGENCY (ESA), 2013, *Sentinel-2 User Handbook*. (Accessed 31 December 2024).

THE EUROPEAN SPACE AGENCY (ESA), Sentinel Online. Available at: https://sentinel.esa.int/ (Accessed 31 December 2024).

TRAGANOS D, POURSANIDIS D, AGGARWAL B, CHRYSOULAKIS N and REINARTZ P, 2018, Estimating Satellite-Derived Bathymetry with the Google Earth Engine and Sentinel-2. *Remote Sensing* 10(6): 859. DOI: https://doi.org/10.3390/rs10060859.

VARDAR D, ERTURAÇ K, ÖZCAN O and GAZIOĞLU C, 2024, Nearshore Seafloor Depositions and Deformations at Paleo-Glacier Active Area revealed from side scan sonar data, case study from Horseshoe Island, Western Antarctica. *EGUsphere* 2024: 1-20.

XU W, JIANG Z, GUO Y, JI X, GUO Z, LIU Y and XIAO X, 2024, Registration of airborne LiDAR bathymetry seafloor point clouds based on the adaptive matching of corresponding points. *IEEE Geoscience and Remote Sensing Letters* 21: 1-5. DOI: 10.1109/LGRS.2024.3366416.

ZHAO J, BARNES B, MELO N, ENGLISH D, LAPOINTE B, MULLER-KARGER F, SCHAEFFER B and HU C, 2013, Assessment of Satellite-Derived Diffuse Attenuation Coefficients and Euphotic Depths in South Florida Coastal Waters. *Remote Sensing of Environment* 131: 38–50. DOI: https://doi.org/10.1016/j.rse.2012.12.009.

Received 18 March 2025
Accepted 8 June 2025